

The Physics of Cometary Anti-tails as Observed in 3I/ATLAS

Eric Keto,¹★ Abraham Loeb,¹

¹Department of Astronomy, Harvard University, 60 Garden Street, Cambridge MA 02138

Accepted XXX. Received YYY; in original form ZZZ

ABSTRACT

Observations of interstellar comet 3I/ATLAS at 3.8 au show an elongated coma similar to a cometary tail but pointing in the direction of the Sun, possibly the first instance of this type of anti-tail which is not a result of perspective. We explain the anti-tail as an anisotropic extension of the snow line, or survival radius of a sublimating ice grain, in the direction of the Sun. The anisotropy is due to the difference in the sublimation mass flux in the solar and perpendicular directions caused by the change in the illumination angle of the cometary surface. The stronger sublimation mass flux in the solar direction results in ice grains with larger sizes, longer sublimation lifetimes, and a snow line at a larger radial distance with respect to other directions. The observed radial surface brightness profiles as a function of illumination angle are well reproduced by a Haser-type radial outflow with constant velocity and sublimating ice grains with angularly dependent survival lengths.

Key words: comets: general, comets: individual: 3I/ATLAS

1 INTRODUCTION

Observations of the interstellar object, 3I/ATLAS, at a distance of 3.8 au from the Sun, by the Hubble Space Telescope (HST) on July 21, 2025 (Jewitt et al. 2025) revealed an anti-tail in the solar direction that is not due to projection. Confirmed by other observations (Tonry et al. 2025; Bolin et al. 2025; Cordiner et al. 2025; Chandler et al. 2025; Seligman et al. 2025), this phenomenon is not common and possibly observed for the first time. In this paper, we explain the development of an anti-tail based on simple physical models of comets.

We model the coma as a radial outflow of sublimating ice grains ejected by gas drag off the cometary surface. Calculated surface temperatures and grain survival times indicate that the sublimation mass flux off the cometary surface must be predominantly CO₂ as observed (Lisse et al. 2025; Cordiner et al. 2025), while the grains must be H₂O ice. The radial extent of the coma depends on the distance that an ice grain survives while sublimating. This snow-line length varies with the solar illumination angle principally through the sublimation mass flux which determines the maximum liftable grain size (Whipple 1951) and the maximum of the grain size distribution. From a chain of simple calculations, we determine the maximum ice-grain size and terminal velocity as a function of the illumination angle to derive the survival length, $\ell = v_\infty t_{\text{life}}$ as a function of illumination angle.

2 THE ANTI-TAIL IN THE HST IMAGE

Figures 1 and 2 show two representations of the HST data. The image is shown with a logarithmic color transfer function. Radial profiles are shown along directions of 10, 100, 190° with respect to the coordinate axes. The profile of 10°, in the direction of the

Sun, is longer than the profiles in the two perpendicular directions at 100 and 190°. None of the profiles fits a single-slope power law as would be expected from a radial dilution of the number density in a constant-velocity, spherical outflow. Their curvature suggests an exponential decrease in the number density with distance from the nucleus as previously mentioned (Jewitt et al. 2025).

We can model the curvature of the radial surface brightness profiles with a Haser-type density law (Haser et al. 2020) that develops from flux conservation in a constant-velocity, spherical outflow combined with destruction of the particles,

$$\frac{1}{r^2} \frac{d}{dr} [r^2 v(a) n(r, a)] = -\frac{n(r, a)}{t_{\text{life}}}. \quad (1)$$

where a is the ice grain size with velocity, $v(a)$ and lifetime t_{life} . The solution for the number density modifies the solution for a steady-state outflow by an exponential,

$$n(r, a) \propto r^{-2} \exp\left(-\frac{r}{\ell(a)}\right). \quad (2)$$

If we select a representative ice grain size to replace the ice-grain size distribution, we can use the same integral solution for the surface brightness as in the original Haser solution for molecular emission. The surface brightness follows,

$$\Sigma(\rho, a) \propto \frac{Q}{4\pi v(a)\rho} 2K_0(x) \quad (3)$$

where ρ is the projected radius, Q is the mass flux of the outflow and K_0 is the modified Bessel function of the second kind, and $x = \rho/\ell(a)$.

Figure 2 shows the mathematical fits to the Haser model,

$$I(x) = C + (A/x) \exp(x/B) \quad (4)$$

where $I(x)$ is the observed counts at coordinate x (pixels) and A, B, C are constants. The fitting is restricted to data that lie above and to

★ E-mail: eketo@cfa.harvard.edu (EK)

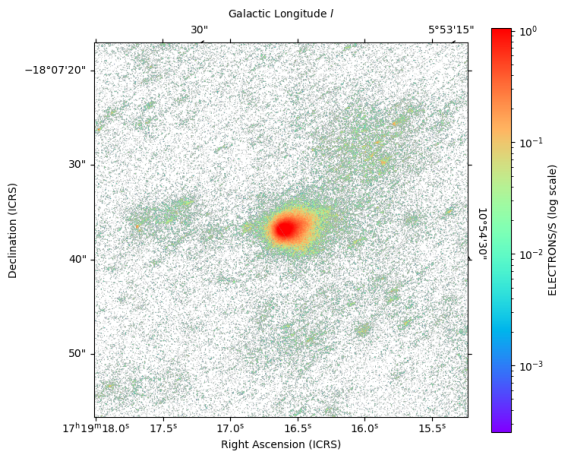


Figure 1. Left: HST image in \log_{10} counts (electrons s^{-1}).

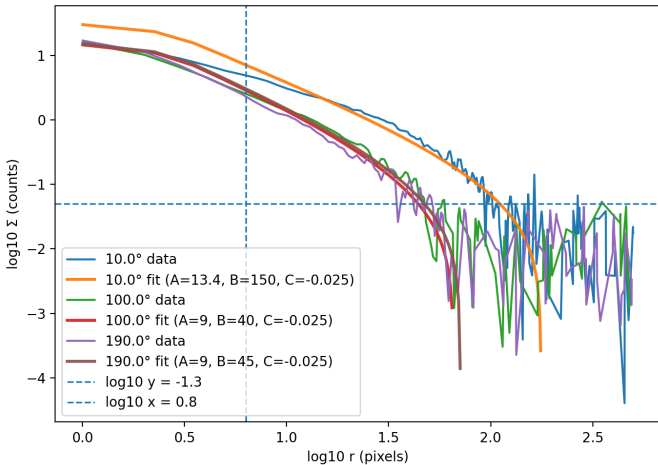


Figure 2. Radial profiles of the surface brightness at angles of 10° , 100° , and 190° where the angles are measured with respect to the x , y coordinate axes. The observed profiles are overlaid with fits to a model Haser-type surface brightness. The x , y axes have units of pixels ($0.04''$) and counts (electrons s^{-1}).

the right of the dashed lines. The horizontal dashed line on figure 1 shows the approximate noise level. The vertical dashed line is placed at three times the resolution of the HST, about 3×2 pixels.

The model curves give an empirical estimate for the lengths, ℓ , of the snow lines in the different directions. At a heliocentric distance of 3.8 au, the apparent length in the solar direction is 3500 km, and 1300 km in the two perpendicular directions. At this distance, the comet is moving toward both the Sun and the Earth with a projection angle of 9.6° and a foreshortening factor of 5.8. Scaling the projected radius, ρ , implies a snow-line length in the solar direction of 29,600 km. The characteristic length of the exponential destruction indicates that volatile ice grains, rather than refractory dust grains, contribute most of the total scattering cross-section in the coma.

The HST observations indicate that the sunward anti-tail from 3I/ATLAS is different from the two more commonly observed anti-tails. Ejection of gas and dust is commonly anisotropic in the direction of the Sun, and particularly active regions of the nucleus can produce jet-like structures directed toward the Sun. Second, the projection of

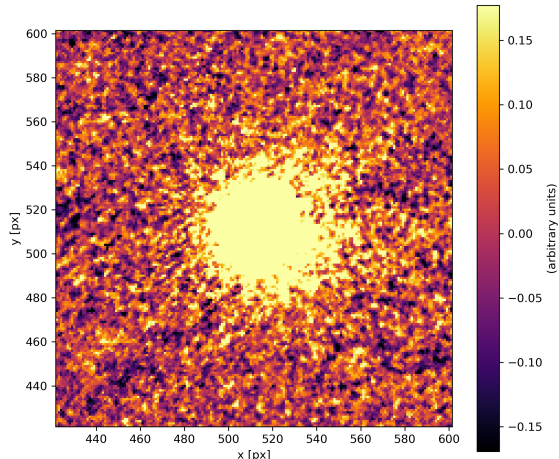


Figure 3. HST image filtered by the rotational-gradient transform with $(\Delta r, \Delta\alpha) = (3, 10)$ (equation 5 showing an absence of small scale anisotropy).

the current position of a coma against a stream of previously ejected dust may place the stream on the sunward side of the coma due to the difference in viewing perspective at the past time of ejection and the current time.

Sunward-directed jets are characteristically narrower, shorter, and fainter than the comae in which they are embedded. Although they can create asymmetry in the larger comae, they may not be easily apparent without image enhancement, for example with the Larson-Sekanina rotational-gradient method of difference imaging (Larson & Sekanina 1984). This filtering is scale dependent according to the spatial separations, $(\Delta r, \Delta\alpha)$, in their equation 1,

$$B'(r, \alpha; \Delta r, \Delta\alpha) = [B(r, \alpha) - B(r - \Delta r, \alpha - \Delta\alpha)] + [B(x, P) - B(x - \Delta x, P + \Delta P)] \quad (5)$$

where B is the image brightness in polar coordinates (r, α) . Application to the HST image, shown in figure 3, finds no anisotropies on the scale of $(\Delta r, \Delta\alpha) = (3, 10)$ (pixels, degrees) as might be expected for a jet-like ejection. The broader anisotropy of the 3I/ATLAS anti-tail begins to show in the differenced image on scales of $(\Delta x, \Delta\alpha) \sim (60, 30)$. This is consistent with the hypothesis that the 3I/ATLAS anti-tail is created by anisotropic destruction by sublimation of the ice grains rather than anisotropic jet emission.

Apparent anti-tails due to projection are sometimes seen when a periodic comet crosses its aphelion orbital point (opposition or true anomaly of 180°). At this point the comet's orbital plane may be seen nearly edge-on. Large dust grains ejected at the comet's previous perihelion passage or passages, whose orbits approximate the comet's, may appear in projection with the comet as narrow sunward tails or necklines. In contrast, 3I/ATLAS is on the incoming leg of its hyperbolic orbit. Furthermore, the exponential decline in the number density of scatterers indicated by the Haser-type surface brightness profiles suggests that the scatterers are destroyed before they have time to wrap around the comet to form a traditional antisolar tail whose remnants might be seen in projection with the coma.

For further comparison, the images of the comet 67P/Churyumov-Gerasimenko analyzed in Rosenbush et al. (2026) illustrate the three types of previously known tails, a traditional dust tail, jet-like ejection revealed by the rotational-gradient filter, and projected necklines. In the 6 October 2021 observations (Fig. 3), comet 67P shows a normal antisolar dust tail ($PA \approx 266^\circ$) and a sunward jet ($PA \approx 127^\circ$) produced by an active area on the nucleus. In the later 6

February 2022 images (Fig. 4), a third feature appears, a bright sunward linear structure identified as a neckline, composed of old dust ejected near perihelion that follows the comet but on a slightly different orbital path. At the same time, two active jets (J1, J2) are seen roughly perpendicular to the Sun-comet vector, representing current outgassing activity. The 3I/ATLAS anti-tail does not fall easily into any one of these categories.

This discussion in this section indicates that the anti-tail from 3I/ATLAS develops from the dependence of the length of the snow line on the illumination angle. So far, we have a mathematical fit for the radial surface brightness in terms of the Haser model that provides estimates of the lengths but not a description of the physics. We now proceed to estimate the snow-line length from physical principles which is the main goal of this study.

3 A PHYSICAL MODEL FOR THE ANTI-TAIL

Theoretically, we expect that the snow line or survival length of a sublimating ice grain of size a , is,

$$\ell(a) = v(a)t_{\text{life}}(a). \quad (6)$$

This suggests a process that results in a longer survival length in the sunward direction. The two factors in the survival length are the velocity of the ice grains and their survival time against sublimation.

The velocity of the ice grains is estimated with the Haser-Whipple (Haser 1957; Whipple 1951) model for free molecular acceleration,

$$a_d = \frac{F_{\text{drag}}}{m_d} = \frac{C_D \pi a^2 v_g J}{\rho_d a} \quad (7)$$

where $C_D \sim 1$ is the drag coefficient; $v_g = \sqrt{8k_B T / (\pi m_g)}$ (m s^{-1}) is the free-expansion gas velocity where $T < 200 \text{ K}$ is the surface temperature; and J is the mass flux ($\text{kg m}^{-2} \text{s}^{-1}$) from sublimation; and ρ_d is the grain density. Integration of the acceleration with some assumptions results in the Probstein terminal velocity (Finson & Probstein 1968),

$$v_\infty \approx \min \left[\sqrt{\frac{3C_D}{2}} \sqrt{\frac{v_g R_n J}{\rho_d a}}, v_g \right]. \quad (8)$$

The radius of the cometary nucleus, R_n , is used as a characteristic length for the acceleration. This estimate requires capping the terminal velocity at the free-expansion speed of the gas, v_g . The terminal velocity scales as $v_\infty \propto J^{1/2} a^{-5/4}$ up to its maximum. This velocity gives us the first of the two factors in the survival length scale $\ell(a) = v_\infty(a)t_{\text{life}}$.

The survival time of a spherical ice grain is proportional to its size,

$$\tau = \frac{m_g}{dm_g/dt} = \frac{\frac{4}{3}a^3 \rho_d}{4\pi a^2 J} = \frac{\rho_d}{3} \frac{a}{J_d} \propto a \quad (9)$$

Here J_d is the sublimation mass flux off the ice grain. The terminal velocity and the lifetimes of the ice grains are now described as a function of the ice grain size.

Ice grain sizes are described by a power-law distribution with an index that is reliably maintained at -3.5 by fragmentation. The maximum ice grain size that can escape the gravitational pull of the nucleus is given by Whipple's maximum liftable grain size. Although this maximum size grain will not actually escape the nucleus since its terminal velocity is zero, we can use this maximum of the grain-size distribution. From the balance between gravity and the drag force.

$$a_{\text{max}} = \frac{3C_D v_g J}{4\rho_d g} \quad (10)$$

where g is the gravitational force of the nucleus, R_n is the nuclear radius, ρ_n is nuclear density, and J is the mass flux off the nucleus. The survival length of larger grains whose terminal velocities are below the maximum of the free-expansion velocity scales as $a^{-1/4}$. For smaller grains that are accelerated to v_g , the maximum velocity, $\ell \propto a$.

The ice grain sizes and hence their lifetimes and also their terminal velocities are both related to the mass flux off the nucleus, J .

The mass flux derives from the energy balance at the surface of the nucleus (Prialnik 2004),

$$(1 - A) \frac{S_0}{r_H^2} \cos(\theta) = \epsilon \sigma T^4 + L_s J - \Gamma \sqrt{\omega/\pi} (T - T_b) \quad (11)$$

where A is the Bond (bolometric) albedo; S_0 is the solar constant at 1 au (1361 W m^{-2}); r_H is the heliocentric distance in au; $\cos(\theta)$ is the illumination factor with θ the illumination or hour angle (HA) around the nuclear circumference and $\theta = 0$ towards the Sun; L_s is the latent heat of sublimation; ω is the angular frequency $2\pi/P$ for period P ; and T_b is the mean equilibrium temperature. T_b is found from the same equation by dropping the last term, replacing $\cos \theta$ by its mean $\langle \cos \theta \rangle \approx 1/\pi$, and solving for T .

The left side of the equation is the power from insolation. The first term on the right side is the radiative cooling. The second is the cooling by sublimation. The third term is the heat flow by conduction from the nuclear interior. This maintains a minimum temperature on the dark side of the nucleus. The form in equation 11 is an approximation of $\kappa \partial T / \partial z$ for radial direction, z . The thermal inertia, Γ , and the thermal conductivity, κ are related as $\Gamma = \sqrt{\kappa \rho_n c_p} = 10 - 60 \text{ (J m}^{-2} \text{ K}^{-1} \text{ s}^{-1/2}\text{)}$, where ρ_n is the nuclear density (Delbo et al. 2015; Groussin et al. 2019, 2025; Boissier et al. 2011).

The mass flux has to satisfy the kinetics at the gas-solid interface described by the Hertz-Knudsen formula,

$$J(T) = \alpha \frac{m_g (P_{\text{vap}}(T) - P_\infty)}{\sqrt{m_g / (2\pi kT)}} \quad (12)$$

where $\alpha \sim 1$ is an accommodation factor.

The calculation of the mass flux, J , is a two-step procedure. The temperature for the surface is obtained from the energy balance with the HK formula for J . The mass flux is then determined for this equilibrium temperature from the HK formula.

If the nucleus is a mixture of components, then we replace the single term, LJ by the sum of terms for the several components. We consider a comet that is 80% H_2O ice and 20% CO_2 ice. Then,

$$LJ = L_{\text{H}_2\text{O}} J_{\text{H}_2\text{O}} f_{\text{H}_2\text{O}} + L_{\text{CO}_2} J_{\text{CO}_2} f_{\text{CO}_2} \quad (13)$$

Figure 4 shows the solutions for each of the pure species and for the mixture. The rapid sublimation of CO_2 cools the surface of the mixture and keeps the temperature of the H_2O too cold for sublimation as previously noted (Lisse et al. 2025). The gas in the coma is then predominantly CO_2 as observed (Lisse et al. 2025; Cordner et al. 2025). Since the surface temperatures are too low for a significant sublimation mass flux of H_2O , the relatively low proportion of gas phase H_2O relative to CO_2 in the coma (Cordner et al. 2025) may derive from the sublimation of the ice grains ejected by gas drag.

The thermal response time scale may be estimated as,

$$\tau(T) = \frac{\Gamma \sqrt{P/\pi}}{4\epsilon \sigma T^4 + \sum f_i L_i dJ/dT} \quad (14)$$

The response time varies from a minimum of 170 s at HA=0 to 3.7 hr at HA=90.0 both shorter than the 16 hour observed rotation period (Santana-Ros et al. 2025; de la Fuente Marcos et al. 2025).

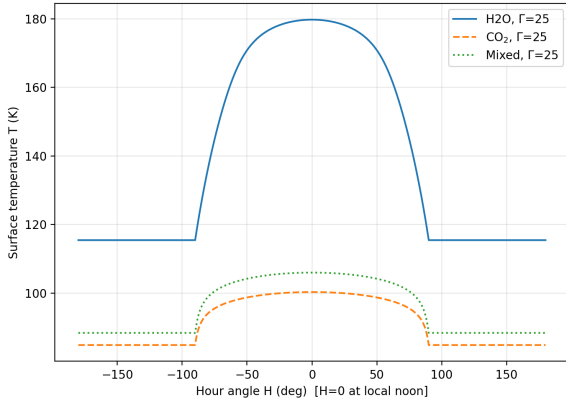


Figure 4. Surface temperature of the nucleus as a function of angle for H_2O , CO_2 , and mixed 80% H_2O 20% CO_2 .

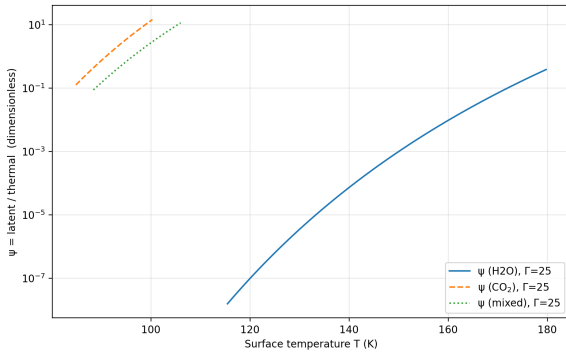


Figure 5. Ratio ψ (equation 19)

The thermal response time scale is longer at lower temperatures. Because of the thermal lag, the temperature on the dark side of the comet will be warmer than its equilibrium temperature. We can estimate the surface temperatures more precisely by including the thermal lag. Written as a finite difference approximation, we estimate the temperature of an equatorial patch of the surface as it rotates with the comet, assuming for convenience a rotation axis perpendicular to the Sun-comet vector (maximum rotation speed),

$$T_{n+1} = T_b(HA_{n+1}) + [T_n - T_{\text{eq}}(HA_{n+1})]e^{\Delta t/\tau_{n+1}} \quad (15)$$

The time series converges immediately to a steady state and is shown in figure 6 for $\Gamma = 25$. For comparison, figure 7 shows the result for $\Gamma = 100$. The difference amounts to an increase in the minimum temperature of 7% on the dark side of the comet.

The solution for the mass flux has two limiting cases depending on whether the cooling is dominated by radiation or sublimation. If $\epsilon\sigma T^4 \ll (1-a)S_0 r^{-2}$, then radiative losses are negligible and most of the solar energy goes into sublimation. Ignoring conduction, the energy-limited mass flux is,

$$J_E \approx \frac{(1-a)S_0}{Lr_H^2} \cos \theta. \quad (16)$$

In this case, the mass flux is independent of temperature.

If the sublimation is limited not by the available energy but by the kinetics at the interface, then $J \approx J_H K$ given by the HK formula. The dependence on T is more complex since the saturation vapor pressure is given by the Clausius-Clapeyron equation,

$$P_{\text{vap}} \approx P_0 \exp(-L/RT). \quad (17)$$

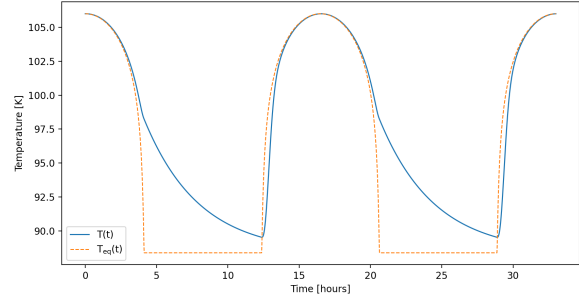


Figure 6. Equilibrium and time-dependent surface temperatures of an equatorial patch of the mixed composition nucleus during two rotations. The thermal inertia, $\Gamma = 25 \text{ J m}^{-2} \text{ K}^{-1} \text{ s}^{-1/2}$.

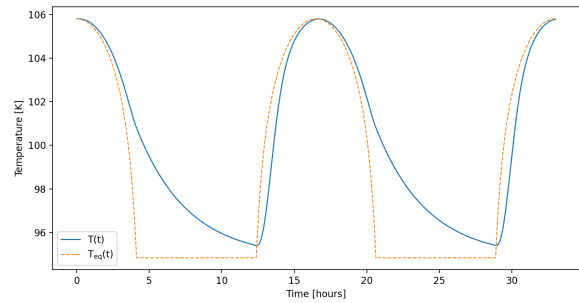


Figure 7. Same as figure 6 but with the thermal inertia, $\Gamma = 100 \text{ J m}^{-2} \text{ K}^{-1} \text{ s}^{-1/2}$.

In this case J has a strong, exponential dependence on temperature, $J \sim T^{-1/2} \exp(-L/RT)$.

We can determine whether the nuclear surface is in the energy or kinetic-limited regime as a function of angle or temperature for a given composition. Define the radiative temperature,

$$T_{\text{rad}} = (F_{\text{abs}}/\epsilon\sigma)^{1/4} \quad (18)$$

where F_{abs} is the absorbed solar flux. For each species define the function,

$$\psi_i = \frac{f_i L_i J_i(T_{\text{rad}})}{F_{\text{abs}}}. \quad (19)$$

If $\Sigma_i \psi_i \gg 1$: energy limited – sublimation cooling dominates $T < T_{\text{rad}}$. J independent of surface T .

If $\Sigma_i \psi_i \ll 1$: kinetic limited – radiation dominates $T \approx T_{\text{rad}}$ and $J \sim T^{-1/2} \exp(L_i/RT)$.

Figure 4 (right) shows that ψ crosses the critical value for CO_2 and for the mixture, but remains < 1 for H_2O for almost the full range of surface temperatures.

Figure 8 shows the length of a representative snow line as a function of hour angle. The figure shows that a representative snow line varies in length by a factor of about seven over the range of hour angle $\pm 90^\circ$. This variation creates the sunward anti-tail.

The maximum of the grain size distribution varies by about two magnitudes as a function of the hour angle. The snow line shown is generated by multiplying the maximum grain size by a constant factor of $f = 10^{-5}$ so that the grain sizes as a function of hour angle are centered around the optical wavelength, $0.5 \mu\text{m}$. Ice grains of this size dominate the total scattering cross-section. Thus the snow line shown is $\ell(HA) = v_{\infty} (fa_{\text{max}}(HA)) t_{\text{life}}(fa_{\text{max}}(HA))$.

Aside from the asymmetry produced by the thermal lag, the curves

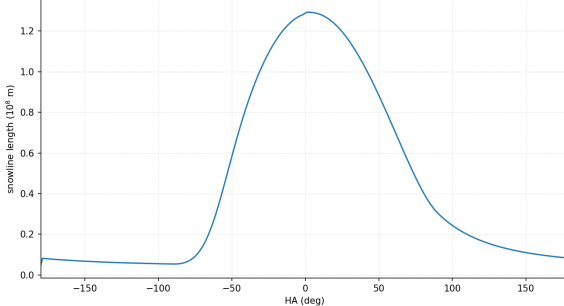


Figure 8. Snow line for water ice as a function of nuclear hour angle for three sizes of ice grains.

for the snow line have the same functional dependence on hour angle as the maximum ice grain size and the sublimation mass flux of CO₂. All are well-fit by a cosine function implicating the illumination angle in the energy balance as the dominant effect on the length of the snow line.

4 DISCUSSION

The model of the anti-tail as a result of the snow-line length in a coma composed of CO₂ gas, H₂O ice grains is an alternative to other hypotheses such as an anti-tail from enhanced ejection of large dust grains followed by fragmentation (Cordiner et al. 2025); from sunward jets (Jewitt & Luu 2025) and/or shaped by solar radiation pressure (Jewitt et al. 2025); or, from anisotropic dust emission from a nucleus with an in-plane rotation pole (Chandler et al. 2025). The snow-line model aligns with other observations. In particular, the surface temperature of the nucleus maintained by the sublimation of CO₂ prevents significant sublimation of H₂O off the nucleus. Instead, the H₂O gas in the coma derives from the sublimation of the ice grains. This allows a comet with a volatile composition of 4:1 H₂O:CO₂ to produce a coma with a 1:8 composition in the gas phase (Keto & Loeb 2025) as observed by the JWST (Cordiner et al. 2025). The snow-line model also allows for the disappearance of the anti-tail at heliocentric distances within ~ 3.5 au where the ice coma collapses due to higher insolation and rapid destruction of the ice grains (Keto & Loeb 2025) as observed (Hoogendam et al. 2025; Fenske 2025).

5 CONCLUSIONS

We compare simple physical models of cometary coma with observations from the Hubble Space Telescope. The Haser-type outflow solution with exponential destruction (equations 1 - 3) provides good fits to the observed surface brightness profiles in the solar and perpendicular directions, indicating that the sublimation of ice grains in the coma, driven by the sublimation mass flux of CO₂ gas from the nucleus, determines the observed curvature of the profiles and the angular anisotropy.

Within a radial model, the anti-tail emerges naturally as a consequence of anisotropic illumination. We find that the angular dependence of the characteristic length scale for the destruction is primarily due to the illumination angle of the cometary surface which affects the sublimation mass flux of CO₂ gas off the cometary surface. The mass flux determines both the terminal velocity of the ice grains and

the maximum size in the grain size distribution and therefore the characteristic survival length of the ice grains in the outflow.

The development of an observable anti-tail depends on a favorable combination of cometary composition and solar insolation that both affect the sublimation mass flux off the cometary surface as well as the destruction of the ice grains by sublimation. In particular, the total scattering cross-section should be dominated by volatile ice grains. The sublimation mass flux and radiation pressure should not be so large as to create a traditional cometary tail, both indicating that an anti-tail is more likely to be observed at larger heliocentric distances. This in turn requires high-angular-resolution observations, such as those of the HST. As 3I/ATLAS approaches the Sun, the physical conditions and shape of the coma will change.

6 ACKNOWLEDGEMENTS

AL was supported in part by the Galileo Project and the Black Hole Initiative. The authors appreciate the help of Prof. D. Jewitt who provided the HST image.

DATA AVAILABILITY

Image data provided courtesy of Prof. D. Jewitt.

REFERENCES

Boissier J., et al., 2011, *A&A*, **528**, A54
 Bolin B. T., et al., 2025, *MNRAS*, **542**, L139
 Chandler C. O., et al., 2025, *arXiv e-prints*, p. arXiv:2507.13409
 Cordiner M. A., et al., 2025, *arXiv e-prints*, p. arXiv:2508.18209
 Delbo M., Mueller M., Emery J. P., Rozitis B., Capria M. T., 2015, in Michel P., DeMeo F. E., Bottke W. F., eds., *Asteroids IV*. pp 107–128, doi:10.2458/azu_uapress_9780816532131-ch006
 Fenske J., 2025, Gemini South Captures Growing Tail of Interstellar Comet 3I/ATLAS During Educational Observing Program, *NOIRLab Press Release No. 2525*, <https://noirlab.edu/public/news/noirlab2525>
 Finson M. L., Probstein R. F., 1968, *ApJ*, **154**, 327
 Groussin O., et al., 2019, *Space Sci. Rev.*, **215**, 29
 Groussin O., et al., 2025, *A&A*, **694**, A21
 Haser L., 1957, *Bulletin de la Societe Royale des Sciences de Liege*, **43**, 740
 Haser L., Oset S., Bodewits D., 2020, *Planet. Sci. J.*, **1**, 83
 Hoogendam W. B., et al., 2025, *arXiv e-prints*, p. arXiv:2510.11779
 Jewitt D., Luu J., 2025, *arXiv e-prints*, p. arXiv:2510.18769
 Jewitt D., Hui M.-T., Mutchler M., Kim Y., Agarwal J., 2025, *ApJ*, **990**, L2
 Keto E., Loeb A., 2025, *arXiv e-prints*, p. arXiv:2510.18157
 Larson S. M., Sekanina Z., 1984, *AJ*, **89**, 571
 Lisse C. M., et al., 2025, *arXiv e-prints*, p. arXiv:2508.15469
 Prialnik D., 2004, in Festou M. C., Keller H. U., Weaver H. A., eds., *Comets II*. University of Arizona Press, pp 359–387
 Rosenbush V., et al., 2026, *Icarus*, **444**, 116799
 Santana-Ros T., et al., 2025, *arXiv e-prints*, p. arXiv:2508.00808
 Seligman D. Z., et al., 2025, *ApJ*, **989**, L36
 Tonry J., et al., 2025, *arXiv e-prints*, p. arXiv:2509.05562
 Whipple F. L., 1951, *ApJ*, **113**, 464
 de la Fuente Marcos R., et al., 2025, *A&A*, **700**, L9

This paper has been typeset from a *TeX/LaTeX* file prepared by the author.